

Scale-Adaptive Power Flow Analysis with Local Topology Slicing and Multi-Task Graph Learning

Yongzhe Li, Lin Guan, *Member, IEEE*, Zihan Cai, Zuxian Lin, Jiyu Huang, Liukai Chen

Abstract—Developing deep learning models with strong adaptability to topological variations is of great practical significance for power flow analysis. To enhance model performance under variable system scales and improve robustness in branch power prediction, this paper proposes a Scale-adaptive Multi-task Power Flow Analysis (SaMPFA) framework. SaMPFA introduces a Local Topology Slicing (LTS) sampling technique that extracts subgraphs of different scales from the complete power network to strengthen the model’s cross-scale learning capability. Furthermore, a Reference-free Multi-task Graph Learning (RMGL) model is designed for robust power flow prediction. Unlike existing approaches, RMGL predicts bus voltages and branch powers instead of phase angles. This design not only avoids the risk of error amplification in branch power calculation but also guides the model to learn the physical relationships of phase angle differences. In addition, the loss function incorporates extra terms that encourage the model to capture the physical patterns of angle differences and power transmission, further improving consistency between predictions and physical laws. Simulations on the IEEE 39-bus system and a real provincial grid in China demonstrate that the proposed model achieves superior adaptability and generalization under variable system scales, with accuracy improvements of 4.47% and 36.82%, respectively.

Index Terms—Power flow analysis, graph learning, cross-scale adaptation, local topology slicing, multi-task learning.

I. INTRODUCTION

DEEP learning-based power flow analysis (DL-based PFA) has emerged as an effective approach to rapidly and accurately evaluate the massive operating scenarios induced by the uncertainty of renewable energy sources [1]. DL-based PFA models typically take bus powers and generator voltages as inputs and generate bus voltage magnitudes and phase angles through nonlinear neural mappings. This direct mapping eliminates the iterative process and complex matrix operations required in traditional numerical methods, offering fast computation [2], [3] and freedom from convergence issues [4]. As DL-based PFA research progresses, the practical applicability of such models in real-world power systems has become a major focus.

Real-world power systems operate in complex and variable scenarios, accompanied by topological changes such as line

This work was supported in part by the Smart Grid-National Science and Technology Major Project of China (2025ZD0804900) and the National Natural Science Foundation of China (No. U22B6007). (Corresponding author: Lin Guan.)

Y. Li, L. Guan, Z. Cai and Z. Lin are with the School of Electric Power, South China University of Technology, Guangzhou 510641, China (e-mail: 10706719873@qq.com; lguan@scut.edu.cn; epc_zihan@mail.scut.edu.cn; 2660910069@qq.com)

J. Huang is with the CSG Energy Development Research Institute Co., Ltd., Guangzhou, 510663, China.

L. Chen is with the Electric Power Research Institute of China Southern Power Grid Company Limited, Guangzhou 510663, China.

switching during maintenance and the integration of new substations and transmission lines during system expansion. Successful application of the DL-based PFA technique in real-world power grids requires further improvements in two aspects: handling varying operation scenarios with high accuracy [5], and addressing changes in grid scale and structure with strong adaptation and generalization.

1) Adaptability to system-scale variations

Foundational work of enhancing model adaptability to topology change includes incorporating power network parameters such as bus self-admittance [6], [7] and branch indices [8] into the input, and applying graph neural networks (GNNs) [9], [10] to interpret power system topologies. Subsequent improvements, such as enlarging the model receptive field [11], [12], [13], [14] and designing physics-based graph convolution kernels [15], further increase the robustness of model performance under varying topologies. Inspired by large language models (LLMs), some studies combined GNNs with Transformer architectures and employed pre-training and fine-tuning to achieve transferable performance across multiple PFA tasks [16]. Nevertheless, existing studies are still limited to cases where line switching is allowed while the number of buses remains fixed.

The ultimate goal of DL-based PFA is to build a general model applicable to power system expansion or even to multiple systems with different topologies and bus scales. Existing studies have shown that although the operation of GNNs is theoretically independent of network size, their accuracy often drops sharply or even fails when the number of buses changes [17]. From the perspective of artificial intelligence, the fundamental reason lies in the distributional shift of graph statistics [18]. There are research works in other fields towards this issue, such as generating synthetic graphs of varying scales to enhance cross-scale adaptability in social network applications [19], adopting subgraph sampling to improve performance on large graphs [20], etc..

Power systems possess inherent local separability that any local subgraph can be regarded as an independent sample for learning. Therefore, extracting subgraphs of different scales from the original power system may be an effective way to enlarge the training set size and diversity, enable the model to learn cross-scale power flow laws, and improve the scale adaptability. However, in power flow analysis, subgraph sampling inevitably leads to inconsistencies in the selection of slack buses, resulting in unaligned reference frames for bus phase angles and increasing the difficulty of learning phase angle mapping.

(2) Accuracy in real-world power systems with multiple voltage levels

Existing DL-based PFA models are typically designed to predict bus voltage magnitudes and phase angles, and then the branch power values are computed using power flow equations [16]. Under this framework, there have been fruitful research works on the enhancement of model accuracy. A widely adopted skill is to embed the physical principles into neural network training [1], [5], [21], [22], [23], [24], [25]. Efforts have been made to incorporate Kirchhoff's current law (KCL) [22], AC power flow equations [23], and operational constraints [24] into loss functions, encouraging the model to follow physical laws while improving accuracy. In [25], a second-order cone relaxation is employed to linearize AC equations, simplifying the learning process and improving precision.

Nonetheless, since most of the studies are tested on standard benchmark systems with idealized impedance parameters, the error amplification phenomenon that exists in real-world power systems with very small impedance branches hasn't been revealed. Such ill-impedance branches result from three-winding transformers, bus switches, etc., and are widely present in real-world power system models, which include multiple voltage levels and the substation bus layouts. During power flow calculation of these low impedance branches, small voltage prediction errors in the DL-based PFA model can be significantly amplified and result in large branch power deviations.

To address the above challenges, this paper proposes a Scale-adaptive Multi-task Power Flow Analysis framework (SaMPFA) to enhance the practical applicability of DL-based PFA. SaMPFA can accommodate power system scale expansion through a Local Topology Slicing (LTS)-based training augmentation and the phase-reference-free design. Also, the proposed model directly predicts all the branch powers, thereby eliminating the error amplification risk in the branch power computation. The main contributions of this paper are summarized as follows:

1) A Reference-free Multi-task Graph Learning (RMGL) model is developed for the DL-based PFA task. Instead of direct phase angle prediction, the RMGL scheme employs the multi-task design to jointly predict the bus voltage and the branch power, which effectively avoids error amplification in the phase-angle-based branch power calculation. Then, the bus phase angle difference can be calculated according to branch-related physical equations. This design also achieves adaptability to the slack bus variations and therefore can support the samples generated by LTS.

2) The LTS-based data augmentation method is proposed, which collects subgraphs of various scales from the power network and populates the training dataset. LTS significantly enriches the topology pattern and scale diversity of samples, therefore improving the adaptability and generalization of the trained PFA model.

3) A group of physics-guided constraints is incorporated to guide the model, including the physical laws of branch angle differences and power losses, which ensures the reliability of the results and improves the accuracy.

4) Comprehensive experiments on a real-world power system with scenarios up to 10% network size variation are

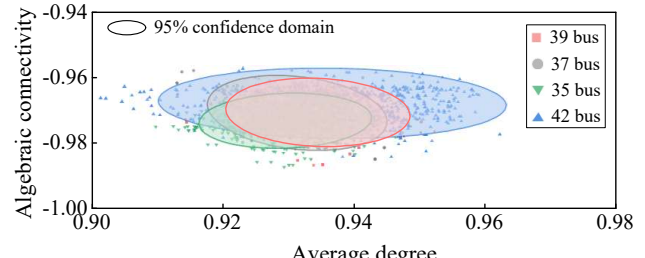


Fig. 1. Distributions of graph characteristics under different bus counts.

carried out. Domain test demonstrates that the proposed model exhibits excellent cross-scale adaptability and generalization capability.

The remainder of this paper is organized as follows. Section II introduces the challenges and framework of SaMPFA. Section III and Section IV describe the structure and training strategy of the RMGL model. Section V presents the case studies, and Section VI concludes the paper.

II. FRAMEWORK DESIGN

A. Key Challenges in Cross-Scale Adaptability

1) Distribution Shifts Caused by Scale Variations

To quantify the impact of variable system scale on graph statistics, the average node degree and algebraic connectivity [26] are selected as the key indicators for the graph topology. The adjacency matrix A is constructed based on the branch reactance, and the Laplacian matrix is obtained as $L = D^{-1/2}AD^{-1/2}$, where D denotes the degree matrix of A . The average degree is the mean of the degree matrix of L , and the algebraic connectivity is the second smallest eigenvalue of L . In Fig. 1, random topology changes are carried out on the IEEE 39-bus system by new station expansion, existing generator shutdown, and line outages. A total of 4,000 network samples with different bus amounts are thus generated, and their distribution in the average node degree and algebraic connectivity feature space is shown in Fig. 1.

It can be observed that the statistical properties of the network exhibit evident shifts related to system bus size. This may explain, from one perspective, why a well-trained PFA model experiences a deterioration in performance when the power grid scale is expanded.

The most straightforward way to enhance the scale adaptability of DL-based PFA models is to augment the training dataset, increase its diversity in both network size and topology. However, a great change in power grid size will lead to a new challenge caused by the slack bus selection. In power flow calculation, a change of the slack bus not only affects the power distribution, but also shifts all the bus phase angles uniformly [27]. From the perspective of the DL model, if the model outputs include bus phase angles, it should learn how slack bus selection affects all the phase angle values, which significantly increases the difficulty in integrated training of variant power system scales.

2) Error Amplification in Branch Power Computation

Existing DL-based PFA models usually follow classic power flow calculation definitions and select bus voltage magnitudes

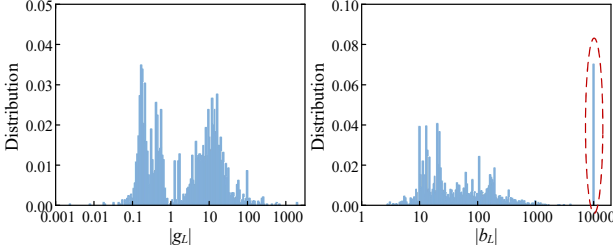


Fig. 2. Per-unit admittance distribution of branches in a real-world power system.

and angles as the direct output. The branch powers are then computed by the following power flow equation [2]:

$$\begin{aligned} \vec{S}_{L,ij} &= \vec{V}_i ((\vec{V}_i - \vec{V}_j) \vec{y}_{L,ij})^* \\ &= \vec{y}_{L,ij}^* (V_i^2 - V_i V_j e^{j\theta_{ij}}) \end{aligned} \quad (1)$$

where \vec{S}_L is the complex branch power, $\vec{V}_i = V_i \angle \theta_i$ and $\vec{V}_j = V_j \angle \theta_j$ are the voltages at bus i and j , and $\theta_{ij} = \theta_i - \theta_j$ is their angle difference. $\vec{y}_L = g_L + j b_L$ is the branch admittance. The superscript $*$ indicates the complex conjugate.

Since DL models cannot perfectly predict all bus voltages, errors in voltages and angles can propagate through (1). To evaluate this, we linearize (1) at an operating point (V_i, V_j, θ_{ij}) :

$$\begin{aligned} \partial S_{L,ij} &= \vec{y}_{L,ij}^* e^{j\theta_{ij}} (2V_i \partial V_i \\ &\quad - e^{j\theta_{ij}} (V_j \partial V_j + V_i \partial V_j + j V_i V_j \partial \theta_{ij})) \end{aligned} \quad (2)$$

$$= K_1 \vec{y}_{L,ij}^* \partial V_i - K_2 \vec{y}_{L,ij}^* \partial V_j - j K_3 \vec{y}_{L,ij}^* \partial \theta_{ij} \quad (3)$$

Since $V_i \approx V_j \approx 1$, the error coefficients are proportional to $|K_1| \approx |K_2| \approx |K_3| \approx 1$. This indicates that the branch power error is approximately proportional to the errors in bus voltages and angle differences, with a ratio of about $|\vec{y}_{L,ij}|$. As shown in Fig. 2, real-world power system models usually contain branches with very low impedance, such as the inclusion of the bus tie switches or the medium-voltage side of three-winding transformers. Since the admittances of such branches can reach 10^3 to 10^4 p.u., even small voltage errors may be amplified, leading to branch power errors greater than 1 p.u..

Towards the above two challenges, a novel design of the DL-based PFA model is proposed in this paper. Direct outputs of the DL-based model are set to be the branch powers, instead of the bus phase angle, which avoids the aforementioned error amplification. Then the phase angle difference of any two buses is calculated by various forms of (1) according to the branch power. Given a phase reference point (the slack bus), the bus phase angles can be easily obtained, which effectively eliminates the difficulty in phase angle prediction caused by the random selection of the slack bus in power grids of different scales.

B. Framework of SaMPFA

1) Architecture

Fig. 3 illustrates the framework of the so-called Scale-adaptive Multi-task Power Flow Analysis (SaMPFA) model proposed in this paper.

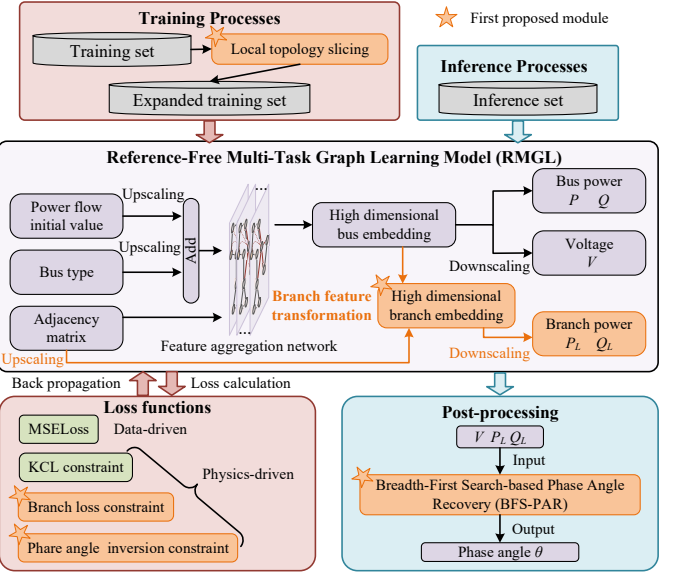


Fig. 3. Framework of SaMPFA.

The kernel of the scheme is the Reference-free Multi-task Graph Learning model (RMGL) in the middle block. In a power system with N buses and E branches, the input of RMGL $\mathbf{X}_{in} \in \mathbb{R}^{N \times 7}$ includes the initial values of active power, reactive power, and voltage magnitudes at all buses, as well as the reactive power bounds and self-admittance. The weighted adjacency matrix \mathbf{A} encodes the branch admittances and tap ratios. To avoid the learning difficulty induced by slack bus changes, phase angles are not explicitly included in either inputs or outputs. The RMGL performs two tasks. The first is a bus-level prediction, which outputs the active power, reactive power, and voltage magnitude of each bus, with the output denoted as $\mathbf{X}_{out} \in \mathbb{R}^{N \times 3}$. The second is a branch-level prediction that outputs the active and reactive power of all branches, with the output denoted as $\mathbf{H}_{out} \in \mathbb{R}^{2E \times 2}$. After feature extraction, the high-dimensional representations of the two terminal buses of each branch are fused and mapped to the branch power through a downscaling network, which significantly enhances numerical robustness.

During training, we adopt Local Topology Slicing (LTS) to sample subgraphs with varying sizes and connection patterns from the full grid. This strategy enlarges the dataset and enriches topological diversity, enabling the model to learn shared physical regularities across different system scales.

The loss function combines data fidelity and physics guidance. In addition to the mean squared loss (MSELoss) and KCL constraint, we introduce an angle restoration constraint to guide learning of branch angle differences, and a branch loss constraint to enforce power transfer and loss relationships. The joint optimization maintains prediction accuracy while preserving physical consistency.

2) Phase Angle Inference and Application

At inference time, the model takes an operating scenario as input and outputs bus active power, reactive power, voltage magnitudes, and branch power for all branches. The phase

Algorithm 1: BFS-based Phase Angle Recovery

Input: Bus voltage magnitudes \mathbf{V} , branch active powers \mathbf{P}_L , branch reactive powers \mathbf{Q}_L , slack bus b_{slack} and its reference angle θ_{slack}

Output: Phase angles θ

- 1 Compute angle differences θ_{ij} across branches by (4)
- 2 Initialize a queue $\mathcal{Q} \leftarrow \{b_{slack}\}$, and the recovered bus set $\mathcal{B}_{visited} \leftarrow \{b_{slack}\}$
- 3 **while** $|\mathcal{B}_{visited}| \neq |\mathcal{B}|$ **do**
- 4 Dequeue a bus b_q from \mathcal{Q}
- 5 Search the neighbor set $\mathcal{N}(b_q)$
- 6 **for** $b_n \in \mathcal{N}(b_q) \setminus \mathcal{B}_{visited}$ **do**
- 7 Recover the angle at b_n : $\theta_n = \theta_q - \theta_{nq}$
- 8 Add b_n to $\mathcal{B}_{visited}$ and enqueue to \mathcal{Q}
- 9 **end for**
- 10 **end while**

angle difference across each branch is computed using (4).

$$\theta_{ij} = \arctan \frac{b_{L,ij}P_{L,ij} + g_{L,ij}Q_{L,ij}}{g_{L,ij}P_{L,ij} - b_{L,ij}Q_{L,ij} - V_i^2(g_{L,ij}^2 + b_{L,ij}^2)} \quad (4)$$

where $P_{L,ij}$ and $Q_{L,ij}$ are the active and reactive power of branch $i - j$.

Based on (4), we propose Breadth First Search-based Phase Angle Recovery (BFS-PAR) to reconstruct bus voltage angles over the entire network. The power system is represented as an undirected graph $\mathcal{G}(\mathcal{B}, \mathcal{E})$, where \mathcal{B} and \mathcal{E} denotes the set of buses and branches. Given a slack bus b_{slack} and its assigned angle θ_{slack} , a BFS strategy is applied to iteratively recover the voltage angles of all buses, as illustrated in Algorithm 1.

III. MODEL DESIGN METHODOLOGY

This section presents the design of the proposed RMGL model. Section III-A describes the structure and computational process of RMGL. Section III-B details the design of the feature extraction network. Section III-C introduces the multi-task design scheme that mitigates the risk of error amplification.

A. Structure of RMGL

To achieve adaptability and generalization under varying system scales, RMGL must be able to recognize and handle changes in the number of buses and branches. Given the strong performance of Graph Transformers [28] in topology recognition and structural generalization, RMGL is built upon this architecture. Its structure is shown in Fig. 4.

Since the self-attention mechanism in Transformers requires inputs of fixed length, RMGL predefines a maximum number of buses, denoted as N_{max} . This design is similar to the maximum token length used in LLMs. When the actual system size N satisfies $N \leq N_{max}$, the model can operate normally. Therefore, N_{max} must be set large enough to cover potential future system scales. For cases where $N < N_{max}$, the remaining $N_{max} - N$ virtual buses are filled with arbitrary values as placeholders in the input features.

It should be noted that changes in the number of buses modify the arrangement of the input feature matrix \mathbf{X}_{in} . To

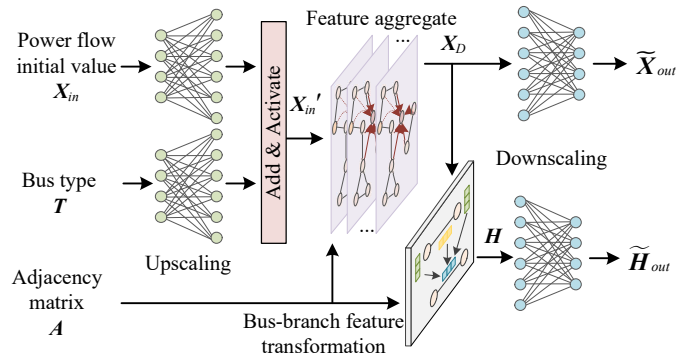


Fig. 4. Structure of RMGL.

reflect the type of each bus and the status of its associated variables, RMGL introduces an additional bus type matrix \mathbf{T} , in addition to the input feature matrix \mathbf{X}_{in} and adjacency matrix \mathbf{A} . The encoding scheme is defined as follows:

- PQ bus: $T_i = [1, 1, 0]$, indicating that active power P and reactive power Q are known, and voltage magnitude V is the target variable.
- PV bus: $T_i = [1, 0, 2]$, where P and V are known, and Q is to be solved. The value 2 for V indicates that its status may change if it switches to the PQ bus due to reactive power limit violations.
- Slack bus: $T_i = [0, 0, 1]$, indicating that voltage magnitude V is known, and both P and Q are to be predicted.
- Virtual bus: $T_i = [0, 0, 0]$, indicating that the bus is a virtual placeholder whose features are masked in subsequent computations.

During the feedforward process, the initial value \mathbf{X}_{in} and the bus type matrix \mathbf{T} are first projected into a high-dimensional feature space, yielding the input embeddings \mathbf{X}'_{in} .

$$\mathbf{X}'_{in} = \sigma(\mathbf{X}_{in}\mathbf{W}_{in} + \mathbf{T}\mathbf{W}_T) \quad (5)$$

where $\mathbf{W}_{in} \in \mathbb{R}^{7 \times d_D}$ and $\mathbf{W}_T \in \mathbb{R}^{3 \times d_D}$ are learnable projection matrices for the initial features and type matrix, $\sigma(\cdot)$ is a nonlinear activation function, and d_D denotes the dimension of the high-dimensional embedding.

Subsequently, an M -layer Masked Graph Transformer (MGT) is used to aggregate features among buses, yielding the high-dimensional power flow representation \mathbf{X}_D :

$$\mathbf{X}_D = f_{MGT}^M(\mathbf{X}'_{in}, \mathbf{A}) \quad (6)$$

Finally, the bus embedding \mathbf{X}_D is passed through a fully connected neural network (FCNN) to generate bus-level power flow predictions. Meanwhile, branch power flows are obtained by extracting branch-level representations \mathbf{H} via a bus-branch feature transformation module, followed by a separate FCNN for output projection.

B. Feature Propagation via Masked Graph Transformer

The Graph Transformer architecture integrates the local topological modeling capability of GNNs with the global feature extraction capability of Transformers. Specifically, the Transformer module employs a multi-head attention (MHA) mechanism to capture dependencies between arbitrary pairs of buses, enhancing generalization to large-scale topologies.

The GNN module aggregates local neighborhood information to extract the structural characteristics of the power grid, enabling the model to handle various network configurations.

Denoted \mathbf{X}_{GT} and \mathbf{X}'_{GT} as the bus embeddings before and after aggregation through the Graph Transformer. The aggregation process is expressed as:

$$\mathbf{X}'_{GT} = f_{MHA}(\mathbf{X}_{GT}) + f_{GNN}(\mathbf{X}_{GT}, \mathbf{A}) + \mathbf{X}_{GT} \quad (7)$$

Since GNNs are inherently capable of managing variations in the number of buses and branches, the Graph Attention Network (GAT) is adopted as the GNN module, whose feed-forward function is defined in [29].

Because the input includes virtual buses that should not participate in feature propagation, a masking mechanism is introduced within the MHA to block them. The attention computation is defined as follows:

$$\alpha^{(k)} = \frac{(\mathbf{X}_{GT} \mathbf{W}_Q^{(k)}) (\mathbf{X}_{GT} \mathbf{W}_K^{(k)})^T}{\sqrt{d_D/K}} \quad (8)$$

$$M_{ij} = \begin{cases} -\infty & i/j \in \mathcal{P} \\ 0 & \text{else} \end{cases} \quad (9)$$

$$f_{MHA}(\mathbf{X}_{GT}) = \parallel^K \text{softmax}(\alpha^{(k)} + \mathbf{M}) (\mathbf{X}_{GT} \mathbf{W}_V^{(k)}) \quad (10)$$

where K is the number of attention heads. $\alpha^{(k)}$ denotes the attention weight matrix for the k -th head. The mask matrix \mathbf{M} is configured such that if either bus i or j is a padded bus, the corresponding entry is set to $-\infty$, ensuring a zero-attention score. $\mathbf{W}_Q^{(k)}$, $\mathbf{W}_K^{(k)}$, and $\mathbf{W}_V^{(k)}$ represent the query, key, and value projection matrices for the k -th head.

Finally, the aggregated features are passed through a feed-forward network (FFN) [30] with nonlinear activation to complete the feature update.

After stacking multiple MGT layers, the model captures both inter-bus dependencies and power grid topological characteristics, yielding the high-dimensional bus representation \mathbf{X}_D . Since the subsequent bus power flow computation no longer depends on other bus features or the system topology, each bus representation $\mathbf{X}_{D,i}$ can be regarded as the complete power flow state of bus i .

C. Design of the Multi-Task Output

To jointly predict bus and branch power flows, RMGL employs a multi-task output architecture. This architecture consists of two task-specific branches that perform feature downscaling and output prediction for buses and branches.

For bus power flow prediction, the high-dimensional bus representation \mathbf{X}_D is mapped to outputs using a fully connected layer:

$$\widetilde{\mathbf{X}}_{out} = \mathbf{X}_D \mathbf{W}_{bus} \quad (11)$$

Branch power flow prediction must satisfy two key physical principles. 1) According to (1), branch power depends only on the states of its two terminal buses and itself, so the transformation must remain localized. 2) Both directions of branch flows must be predicted simultaneously to support physical consistency constraints.

For a branch l connecting buses $i \rightarrow j$, the power prediction is formulated as:

$$\mathbf{H}_l = (\mathbf{X}_{D,i} \parallel \mathbf{X}_{D,j} \parallel (\mathbf{X}_{D,i} - \mathbf{X}_{D,j}) \parallel \mathbf{A}_{ij} \mathbf{W}_A) \mathbf{W}_H \quad (12)$$

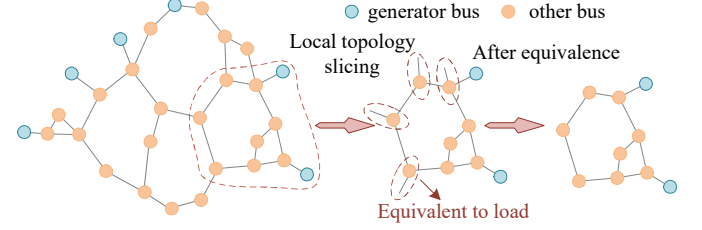


Fig. 5. Local topology slicing.

$$\widetilde{\mathbf{H}}_{out,l} = \mathbf{H}_l \mathbf{W}_{branch} \quad (13)$$

where $\mathbf{W}_A \in \mathbb{R}^{3 \times d_D}$ is the branch-level feature projection matrix. $\mathbf{W}_H \in \mathbb{R}^{4d_D \times d_D}$ is the branch feature extraction matrix, which derives representative features from both the terminal buses and the branch itself. $\mathbf{W}_{branch} \in \mathbb{R}^{d_D \times 2}$ is the projection matrix used to map the extracted features to the final power flow outputs. The above formulation is sensitive to the bus order, allowing directional prediction at both ends of the branch. This property lays the foundation for the physics-informed constraints introduced later.

IV. TRAINING AND EVALUATION

This section presents the training and evaluation strategy of the proposed model. Section IV-A introduces the LTS method for training data augmentation. Section IV-B analyzes the potential violations of physical laws in existing training strategies and develops a more comprehensive hybrid loss function. Section IV-C describes the evaluation metrics, focusing on the maximum error of each test sample.

A. Training Sample Augmentation Based on LTS

The topology of a power system can be represented as a graph \mathcal{G} . By extracting subgraphs \mathcal{G}_{sub} of arbitrary scales from the complete topology, the distributions of bus and branch power flows within each subgraph still satisfy the power flow equations. Therefore, any local topology of the grid can be regarded as an independent sample for model learning.

As shown in Fig. 5, the LTS method extracts subgraphs with different bus numbers and connection patterns, significantly enhancing both the quantity and diversity of training samples. The extraction follows two basic principles:

- Each subgraph must include at least one generator bus to ensure power balance.
- The power on boundary tie lines must be equivalently represented as load injections to maintain consistency with the original grid.

The core procedure of LTS is as follows:

- 1) Randomly select a starting bus and expand the subgraph based on the adjacency matrix until the target number of buses is reached.
- 2) Replace the power of tie lines outside the subgraph with equivalent loads to preserve power flow consistency.
- 3) Introduce power perturbations and branch outages to generate samples with diverse flow distributions.

This sampling method, combining topological and power perturbations, can produce an almost unlimited number of training samples even from limited original data, thereby improving the structural coverage of the training set.

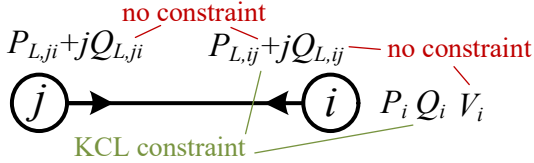


Fig. 6. Model outputs and their physical constraints.

B. Data-Physics Joint Driven Loss Function

Existing DL based PFA studies typically combine MSELoss with KCL constraints [22]. However, within SaMPFA, relying solely on KCL is insufficient to ensure full physical consistency. As shown in Fig. 6, KCL only enforces local power balance between buses and adjacent branches but does not constrain branch end differences or the relation between branch power and bus voltage. Therefore, additional physical mechanisms are incorporated to guide the model toward better adherence to physical laws.

To achieve both numerical accuracy and physical consistency, a hybrid loss function is defined as:

$$\mathcal{L} = \varepsilon_{data} \mathcal{L}_{data} + \varepsilon_{phy} \mathcal{L}_{phy} \quad (14)$$

where ε_{data} and ε_{phy} are the weighting factors for the data-driven loss and physics-driven loss.

1) Data-Driven Loss

The data-driven term consists of weighted mean-squared errors at both bus and branch:

$$\mathcal{L}_{data} = \frac{\varepsilon_N}{B} \sum_b^B \left\| \widetilde{\mathbf{X}}_{out}^{(b)} - \mathbf{X}_{out}^{(b)} \right\|^2 + \frac{\varepsilon_E}{B} \sum_b^B \left\| \widetilde{\mathbf{H}}_{out}^{(b)} - \mathbf{H}_{out}^{(b)} \right\|^2 \quad (15)$$

where B is the number of training samples, and b is the sample index. ε_N and ε_E are the weights for bus and branch-level prediction errors.

2) Physics-Driven Loss

To improve the physical consistency of the model outputs, we introduce the KCL constraint, branch loss constraint, and angle reconstruction constraint into the loss function.

KCL constraint \mathcal{L}_{KCL} minimizes bus unbalanced power to ensure compliance with Kirchhoff's Current Law:

$$\mathcal{L}_{KCL} = \frac{1}{B} \sum_b^B \sum_i^{N^{(b)}} \left(\Delta \widetilde{P}_i^{(b)} + \Delta \widetilde{Q}_i^{(b)} \right) / N^{(b)} \quad (16)$$

$$\left\{ \begin{array}{l} \Delta \widetilde{P}_i = \left| \widetilde{P}_i + \sum_{j \in \mathcal{N}(i)} \left(\widetilde{P}_{L,ij} + \widetilde{V}_i^2 g_{m,ij} \right) \right| \\ \Delta \widetilde{Q}_i = \left| \widetilde{Q}_i + \sum_{j \in \mathcal{N}(i)} \left(\widetilde{Q}_{L,ij} - \widetilde{V}_i^2 b_{m,ij} \right) \right| \end{array} \right. \quad (17)$$

where $N^{(b)}$ is the number of buses in sample b . $\Delta \widetilde{P}_i^{(b)}$ and $\Delta \widetilde{Q}_i^{(b)}$ are the active and reactive power imbalances at bus i . $\mathcal{N}(i)$ is the set of neighbors of bus i . $g_{m,ij}$ and $b_{m,ij}$ are the shunt conductance and susceptance of branch l .

Branch loss constraint \mathcal{L}_{loss} compares the predicted branch losses with the physical losses calculated from predicted voltages and currents to ensure power conservation:

$$\widetilde{I}_{ij} = \sqrt{\widetilde{P}_{L,ij}^2 + \widetilde{Q}_{L,ij}^2} / \widetilde{V}_i \quad (18)$$

$$\widetilde{P}_{loss,ij} = \left| \widetilde{I}_{ij}^2 r_{L,ij} \right|, \widetilde{Q}_{loss,ij} = \left| \widetilde{I}_{ij}^2 x_{L,ij} \right| \quad (19)$$

$$P_{loss,ij} = |P_{L,ij} + P_{L,ji}|, Q_{loss,ij} = |Q_{L,ij} + Q_{L,ji}| \quad (20)$$

$$\begin{aligned} \mathcal{L}_{loss} = & \frac{1}{B} \sum_b^B \sum_{l=(i,j)}^{2E^{(b)}} \frac{\left| \widetilde{P}_{loss,ij}^{(b)} - P_{loss,ij}^{(b)} \right|}{2E^{(b)}} \\ & + \frac{1}{B} \sum_b^B \sum_{l=(i,j)}^{2E^{(b)}} \frac{\left| \widetilde{Q}_{loss,ij}^{(b)} - Q_{loss,ij}^{(b)} \right|}{2E^{(b)}} \end{aligned} \quad (21)$$

where \widetilde{I}_{ij} is the current computed from the predicted branch power flow. $r_{L,ij} + jx_{L,ij} = 1/(g_{L,ij} + jb_{L,ij})$ is the branch impedance. $P_{loss,ij}$ and $Q_{loss,ij}$ are the predicted active and reactive power losses on branch l . $E^{(b)}$ is the number of branches in sample b .

Angle reconstruction constraint \mathcal{L}_{angle} uses (4) to estimate angle differences from predicted branch powers and voltages, guiding the model to learn their physical patterns:

$$\mathcal{L}_{angle} = \frac{1}{B} \sum_b^B \sum_{l=(i,j)}^{2E^{(b)}} \left| \widetilde{\theta}_{ij}^{(b)} - \theta_{ij}^{(b)} \right| / 2E^{(b)} \quad (22)$$

Finally, the physics-driven loss is a weighted sum of the above three components, where ε_{KCL} , ε_{loss} , and ε_{angle} are the weights for each constraint term.

$$\mathcal{L}_{phy} = \varepsilon_{KCL} \mathcal{L}_{KCL} + \varepsilon_{loss} \mathcal{L}_{loss} + \varepsilon_{angle} \mathcal{L}_{angle} \quad (23)$$

C. Evaluation Method Focused on Extreme Errors

Most studies focus on average prediction errors across all buses and branches. However, in PFA, a single large deviation can compromise the reliability of the entire sample. Therefore, the maximum error per sample deserves greater attention.

For each test sample, the maximum errors of voltage magnitude, phase angle, branch power, and bus unbalanced power are denoted as E_V , E_θ , E_{SL} , and $E_{\Delta S}$. For example, the average maximum error of voltage magnitude is defined as:

$$\overline{E}_V = \frac{1}{B_t} \sum_{b=1}^{B_t} E_V^{(b)} = \frac{1}{B_t} \sum_{b=1}^{B_t} \max_i \left| \widetilde{V}_i^{(b)} - V_i^{(b)} \right| \quad (24)$$

where B_t is the number of samples in the test set.

In addition, we define an accuracy indicator Acc , representing the percentage of samples where all prediction errors fall below predefined thresholds:

$$Acc = \frac{1}{B_t} \sum_{b=1}^{B_t} \mathbb{I} \left(E_V^{(b)} \leq \mu_V, E_{SL}^{(b)} \leq \mu_{SL}, E_{\Delta S}^{(b)} \leq \mu_{\Delta S} \right) \quad (25)$$

where $\mathbb{I}(\cdot)$ is the indicator function. The thresholds of E_V , E_{SL} , and $E_{\Delta S}$, denoted as μ_V , μ_{SL} , and $\mu_{\Delta S}$, are set to 0.01p.u., 10 MVA, and 10 MVA.

V. CASE STUDY

This section demonstrates the effectiveness of the proposed method in both the IEEE 39-bus system and a real-world provincial power grid in China.

A. Sample Generation

1) Case I: IEEE 39-Bus System

The system consists of 39 buses and 46 branches. Initially, 8,760 baseline operating scenarios are generated by

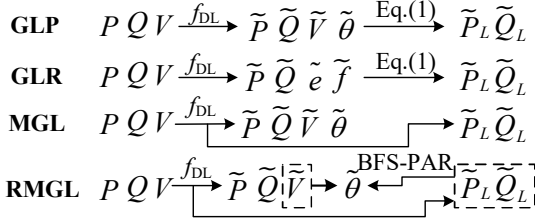


Fig. 7. Output designs of different models.

considering 0-3 generator outages or the addition of 1-2 new buses. From these, 5,000 scenarios are randomly selected, and a training set with 1 million samples is created using the LTS method described in Section IV-A. Furthermore, 3,000 additional baseline scenarios are selected, and 20% fluctuations in bus power, along with 0-2 branch outages, are considered, generating a test set, a downscaled generalization set (Gen-D), and an upscaled generalization set (Gen-U), each with 100,000 samples. It is noted that, during the generation of Gen-D and Gen-U, the number of buses in the system is modified to 35 and 42, respectively. These configurations have not been seen in the training set, thereby serving to evaluate the model's generalization ability across different system scales.

2) Case II: Real-World Provincial Power Grid

Using 366 days of operational data from a provincial power grid, 8,784 baseline scenarios are constructed. The first 300 days of data are divided into training and testing sets with a 4:1 ratio, producing 500,000 and 100,000 samples, respectively, following the same procedure as Case I. The remaining 66 days form the generalization set (Gen set), generating about 150,000 samples. The bus counts of the training, testing, and generalization sets range from 300-687, 633-686, and 634-690, respectively. Within the Gen set, 25,944 samples contain buses unseen during training and are defined as Gen-U, while the remaining 124,065 samples constitute the normal generalization set (Gen-N).

B. Training Strategy

The model is built on the MindSpore framework, with training carried out on 32 Ascend 910B NPU cores, while inference is performed on 8 NPUs. Due to the large magnitude of angle reconstruction and branch loss in the early training stage, a two-stage training strategy is adopted. *In the first stage*, only the data-driven loss and KCL constraint are used. The loss weights are set as: $\varepsilon_{data} = 1$, $\varepsilon_{phy} = 0.3$, $\varepsilon_N = 1$, $\varepsilon_E = 5$, $\varepsilon_{KCL} = 0.5$. *In the second stage*, angle reconstruction and branch loss terms are added, with weights $\varepsilon_{loss} = 0.1$, $\varepsilon_{angle} = 3$. The number of training epochs for the two stages is 200/1000 for Case II, and 200/200 for Case I.

C. Verification of the Framework Design

This section validates the advantages of the proposed framework through comparative experiments. Following the common output design strategies in existing DL-based PFA studies, three baseline models are constructed:

- GLP (Graph Learning under Polar coordinate): A single-task model that outputs the voltage magnitude and phase

TABLE I
PERFORMANCE COMPARISON IN CASE I

Dataset	Model	Acc (%)	E_V ($\times 10^{-3}$ p.u.)	E_θ ($\times 10^{-2}$ °)	E_{SL} (MVA)	$E_{\Delta S}$ (MVA)
Test set	GLP	99.54	0.25	2.68	0.80	1.03
	GLR	99.63	0.25	3.14	0.91	0.90
	MGL	99.64	1.11	3.90	0.73	0.67
	RMGL	99.87	0.62	1.88	0.43	0.43
Gen-D	GLP	98.74	0.62	5.87	1.28	1.39
	GLR	98.79	0.66	6.68	1.50	1.31
	MGL	98.53	1.40	6.26	1.21	1.09
	RMGL	99.29	0.78	3.15	0.73	0.69
Gen-U	GLP	63.98	6.40	3.84	14.12	9.21
	GLR	66.87	5.38	4.78	9.59	7.24
	MGL	66.18	6.42	6.50	5.21	3.86
	RMGL	82.42	3.38	3.48	3.93	2.47

TABLE II
PERFORMANCE COMPARISON IN CASE II

Dataset	Model	Acc (%)	E_V ($\times 10^{-3}$ p.u.)	E_θ ($\times 10^{-2}$ °)	E_{SL} (MVA)	$E_{\Delta S}$ (MVA)
Test set	GLP	50.72	2.14	66.42	22.94	3.65
	GLR	47.09	2.13	72.14	33.49	9.30
	MGL	96.07	4.75	14.43	2.94	4.01
	RMGL	99.28	3.11	8.80	1.65	2.22
Gen set (Gen-N & Gen-U)	GLP	46.66	2.81	75.89	25.93	3.40
	GLR	39.59	2.25	88.89	39.02	9.38
	MGL	90.73	5.88	19.25	3.73	4.58
	RMGL	97.98	3.59	11.48	2.10	2.59

angle in polar coordinates. Its input and output design follows the same configuration as in [11].

- GLR: A single-task model that outputs the real and imaginary parts of bus voltages in rectangular coordinates, consistent with the output design in [23].
- MGL: A variant of RMGL that additionally includes the bus phase angle as both input and output variables.

All three models are built under a fixed reference frame. Their output designs are illustrated in Fig. 7, where e and f denote the real and imaginary parts of the bus voltages.

To ensure fairness, the four models are trained with identical training samples, input features, and feature extraction networks. Their performances in Case I and Case II are summarized in Table I and Table II.

The comparison yields the following insights:

- 1) When the bus angle is included in the output (MGL), the model struggles to learn absolute angles, especially in Case II. This difficulty also affects the learning of other variables.
- 2) Compared with single-task models (GLP and GLR), the proposed multi-task framework effectively suppresses error amplification. As shown in Table I, GLP and GLR exhibit voltage and angle errors of about 6×10^{-3} p.u. and 4×10^{-2} ° in Gen-U. These small errors are magnified by the power flow equations, leading to branch power errors up to 10 MVA. The problem becomes more severe in Case II, particularly in real-world networks with many low-impedance branches. By contrast, the proposed multi-task design reduces error propagation and significantly improves the accuracy of branch power prediction.

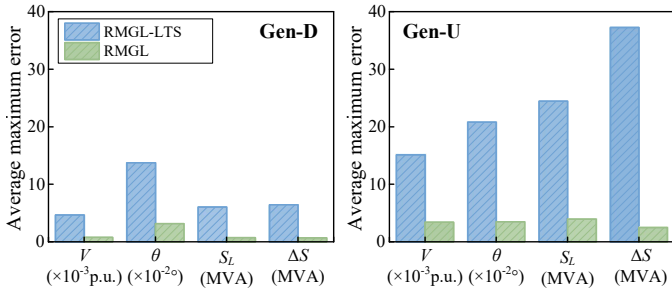


Fig. 8. Effect of LTS in Case I.

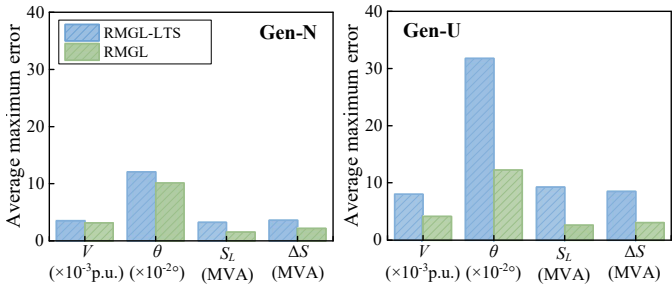


Fig. 9. Effect of LTS in Case II.

D. Effect of LTS on Scale Adaptability

To evaluate the impact of the LTS on training effectiveness, a comparative experiment is conducted. In the sample generation, training samples are generated without using LTS, considering only bus power fluctuations and branch outages for data augmentation. This sample construction approach is similar to that in [16], [22]. The model is trained on 1 million samples and is denoted as RMGL-LTS.

As shown in Fig. 8, the model trained without LTS exhibits significantly higher prediction errors in Case I, particularly in the Gen-U dataset. This is because grid expansion introduces notable shifts in graph characteristics, while the model without LTS is only exposed to systems containing 36-41 buses during training. The limited exposure to diverse topologies causes partial overfitting and poor generalization to unseen system scales.

In Case II, the same conclusion holds. Although the training set includes systems with 632-687 buses, allowing the model to learn some general power flow patterns across different scales, its topological diversity remains insufficient compared with the LTS-based training. As shown in Fig. 9, the performance improvement from LTS in the Gen-N dataset is moderate; however, when the grid contains unseen structures, the difference becomes significant. LTS reduces the prediction errors of the four electrical quantities by 48.31%, 61.50%, 71.68%, and 64.16%, respectively, demonstrating that it substantially enhances model adaptability and generalization capability under system-scale variations.

To further investigate the influence of LTS on the distribution of graph features in training samples, the distributions of the training set, Gen-D, and Gen-U in Case I are visualized, as shown in Fig. 10. Without LTS, the training distribution is narrow, with large overlap between the training set and Gen-D but limited overlap with Gen-U, resulting in inferior performance on Gen-U. After introducing LTS, the training

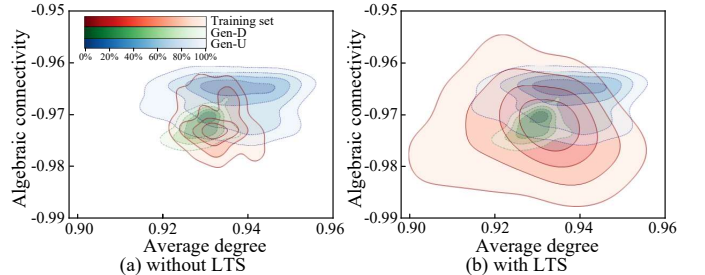


Fig. 10. Graph structure distribution of datasets.

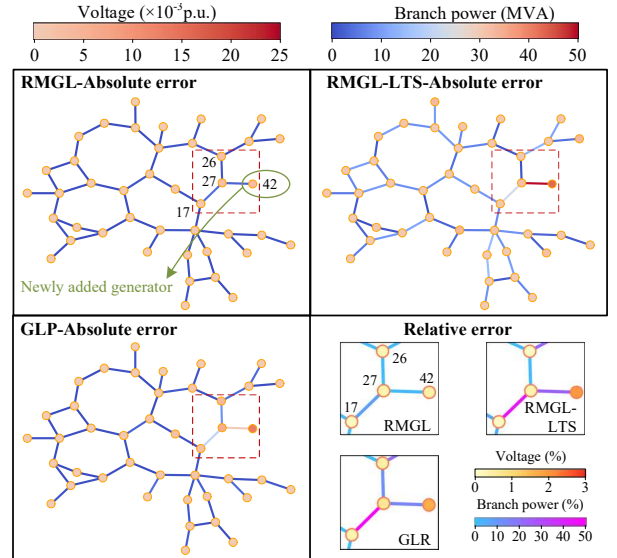


Fig. 11. Performance on an expansion sample in Case I.

distribution expands significantly, fully covering Gen-D and most of Gen-U, thereby greatly improving model performance across both datasets.

E. Analysis of Expansion Scenarios

To evaluate the adaptability of the proposed method to grid expansion, one expansion scenario from Case I is examined, where a new generator bus #42 is connected to bus #27. As shown in Fig. 11, when the system is expanded, RMGL-LTS and GLP perform poorly in the local area around the new bus, particularly in branch power prediction. Their maximum branch errors are 44.70 MVA and 27.63 MVA higher than the proposed model. For example, on branch #17-#27 with an actual power flow of 57.31 MVA, the prediction errors of RMGL, RMGL-LTS, and GLP are 8.08%, 46.02%, and 39.32%, respectively. These results demonstrate that the proposed model exhibits stronger adaptability to topological changes.

From a theoretical perspective, RMGL-LTS is trained only on networks with 36-41 buses, which weakens its ability to generalize when the number of buses increases. Although GLP benefits from LTS and performs better than RMGL-LTS, its output design couples bus voltages and branch powers too tightly. As shown in Fig. 11, the relative errors of voltages at buses #17 and #27 are both below 0.70%. However, due to error amplification in the branch flow equations, the power

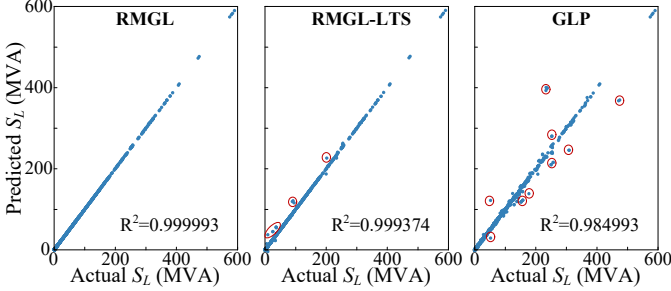


Fig. 12. Actual and predicted branch powers in an unseen scenario of Case II.

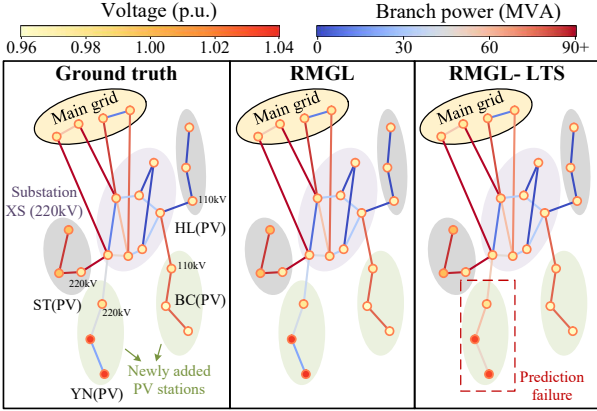


Fig. 13. Prediction results for the local area with newly added PV stations.

error on branch #17-#27 reaches 39.32%. By decoupling bus voltages and branch powers, the proposed multi-task architecture achieves greater stability under system expansion.

The same test is conducted using a scenario from Case II that includes two newly added photovoltaic (PV) stations. The three models predict the power flows of all branches. As shown in Fig. 12, the proposed model achieves the best performance, with predicted branch powers closely matching actual values across the system.

We also compare prediction accuracy in the expanded local topology. Since RMGL-LTS does not use LTS, it shows poor accuracy in unseen topologies. As shown in Fig. 13 two new PV stations (#YN and #BC) are connected to different buses of the 220 kV substation #XS. While RMGL-LTS correctly predicts the power of #BC, it produces a large error at #YN, predicting 49.82 MVA instead of the actual 20.35 MVA. In contrast, the proposed model provides accurate predictions in this region, highlighting the role of LTS in improving adaptability to real-world grid expansion.

Compared with GLP, the proposed model shows clear advantages in predicting lines within the substation. As shown in Fig. 14, both models predict voltages accurately in the substation. However, due to the low impedance of the medium-voltage side of the three-winding transformer, STP suffers severe error amplification, leading to a branch error as large as 90 MVA. This error propagates through the KCL constraint, reducing accuracy in adjacent branches. By decoupling bus voltage and branch power outputs, the proposed design prevents error propagation and significantly improves branch power prediction reliability.

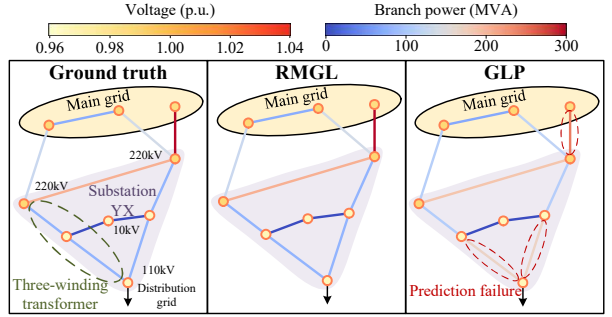


Fig. 14. Prediction results for lines inside the substation.

TABLE III
PHYSICAL CONSTRAINT VIOLATIONS IN CASE I

\mathcal{L}_{loss}	\mathcal{L}_{angle}	Test set (36-41 buses)			Gen set (35&42 buses)		
		P_{loss} (MW)	Q_{loss} (MVar)	$\Delta\theta$ ($\times 10^{2\circ}$)	P_{loss} (MW)	Q_{loss} (MVar)	$\Delta\theta$ ($\times 10^{2\circ}$)
×	×	0.07	0.26	1.28	0.42	1.22	3.31
✓	×	0.06	0.22	1.08	0.09	0.58	3.16
×	✓	0.06	0.23	0.91	0.34	0.90	2.02
✓	✓	0.06	0.21	0.94	0.09	0.61	1.98

F. Hybrid Loss Function Enhances Physical Consistency

This section evaluates the effect of branch loss and angle difference constraints on the physical consistency of model outputs through ablation experiments. Four test settings are conducted in both case studies, and the results are reported in Table III and Table IV. With the branch loss constraint \mathcal{L}_{loss} , the physical consistency of active and reactive power between branch terminals improves significantly, reducing branch loss errors by 61.91% and 45.14% in the two systems. The angle difference constraint \mathcal{L}_{angle} effectively reduces angle errors, which improves the accuracy of branch power prediction and decreases errors in the BFS-PAR recovery process. When both constraints are applied together, the model combines the benefits of each, leading to tighter alignment between outputs and physical equations.

G. Model Initialization Improves NR Convergence

Finally, the effect of model outputs on the convergence of the Newton-Raphson (NR) method is investigated. By increasing system load levels, 20,000 test samples are generated in both systems. The NR method is first initialized with a flat start, and the convergence status, average iteration counts of all samples, and runtime are recorded (with a maximum of 200 iterations). The proposed model is then used to infer bus voltages and angles, which are employed as the initial state of NR, and the same data are recorded.

As shown in Table V, initializing NR with DL model outputs significantly improves convergence. In Case II, the convergence rate increases by 40.16%. The number of NR iterations is also greatly reduced, leading to runtime improvements of 16.18% and 20.13% in the two systems. Considering DL inference alone, the proposed model achieves speedups of 535 \times and 233 \times compared with NR, making it a superior choice for rapid online analysis of large sample sets.

TABLE IV
PHYSICAL CONSTRAINT VIOLATIONS IN CASE II

\mathcal{L}_{loss}	\mathcal{L}_{angle}	Test set			Gen set		
		P_{loss} (MW)	Q_{loss} (MVar)	$\Delta\theta$ ($\times 10^2$)	P_{loss} (MW)	Q_{loss} (MVar)	$\Delta\theta$ ($\times 10^2$)
×	×	0.92	0.76	8.84	1.18	0.91	11.97
✓	×	0.40	0.51	7.43	0.44	0.74	10.64
×	✓	0.79	0.59	4.13	0.83	0.75	7.37
✓	✓	0.44	0.52	4.28	0.46	0.68	6.34

TABLE V
IMPACT OF MODEL INITIALIZATION ON NR CONVERGENCE

Case	Method	Convergence rate(%)	Iterations	DL time(s)	NR time(s)
I	NR	100%	5.313	/	578.21
	DL+NR	100%	2.001	1.08	484.65
II	NR	54.19%	78.821	/	4813.43
	DL+NR	94.35%	9.642	20.70	3844.44

VI. CONCLUSION

This paper presents a novel SaMPFA framework to enhance the applicability of DL models in real-world power systems. By optimizing both model architecture and training strategy, the proposed approach achieves strong adaptability and accuracy across varying system scales and complex topologies. Experiments on the IEEE 39-bus system and a real provincial grid lead to the following conclusions:

1) SaMPFA achieves superior adaptability and generalization under system-scale variations. Accuracy improves by 0.27%/8.67% for seen and unseen scales in the IEEE 39-bus system, and by 34.65%/38.99% in the real-world system, confirming its scalability.

2) LTS effectively enhances the diversity of graph features, improving model robustness in grid expansion scenarios. The RMGL model exhibits higher stability and accuracy in branch power prediction, especially in real-world systems.

3) Using RMGL predictions as initialization significantly accelerates numerical power flow convergence, reducing iterations by 37.62% in the IEEE 39-bus system and improving convergence rate by 40.16% in the real-world system.

This study represents a first step toward building a general PFA model adaptable to diverse power systems. Future work will extend the SaMPFA framework for multi-system joint training and rapid transfer to unseen systems.

REFERENCES

- [1] M. Bento, "Physics-guided neural network for load margin assessment of power systems," *IEEE Trans. Power Syst.*, vol. 39, no. 1, pp. 564-575, Jan. 2024.
- [2] Y. Yang, Z. Yang, J. Yu, B. Zhang, Y. Zhang and H. Yu, "Fast calculation of probabilistic power flow: a model-based deep learning approach," *IEEE Trans. Smart Grid*, vol. 11, no. 3, pp. 2235-2244, May 2020.
- [3] Q. Gao, *et al.*, "Model-driven architecture of extreme learning machine to extract power flow features," *IEEE Trans. Neural Netw. Learn. Syst.*, vol. 32, no. 10, pp. 4680-4690, Oct. 2021.
- [4] S. Okhuegbe, A. Ademola and Y. Liu, "Newton-raphson ac power flow convergence based on deep learning initialization and homotopy continuation," *IEEE Trans. Ind. Appl.*, vol. 61, no. 2, pp. 2037-2046, Mar./Apr. 2025.
- [5] X. Hu, H. Hu, S. Verma and Z.-L. Zhang, "Physics-guided deep neural networks for power flow analysis," *IEEE Trans. Power Syst.*, vol. 36, no. 3, pp. 2082-2092, May 2021.
- [6] Y. Du, F. Li, J. Li and T. Zheng, "Achieving 100x acceleration for n-1 contingency screening with uncertain scenarios using deep convolutional neural network," *IEEE Trans. Power Syst.*, vol. 34, no. 4, pp. 3303-3305, Jul. 2019.
- [7] B. Tan, J. Zhao and Y. Chen, "Scalable risk assessment of rare events in power systems with uncertain wind generation and loads," *IEEE Trans. Power Syst.*, vol. 40, no. 2, pp. 1374-1388, Mar. 2025.
- [8] M. Xiang, J. Yu, Z. Yang, Y. Yang, H. Yu and H. He, "Probabilistic power flow with topology changes based on deep neural network," *Int. J. Electr. Power Energy Syst.*, vol. 117, p. 105650, May 2020.
- [9] X. Hu, *et al.*, "Adaptive power flow analysis for power system operation based on graph deep learning," *Int. J. Electr. Power Energy Syst.*, vol. 161, p. 110166, Oct. 2024.
- [10] M. Yang, G. Qiu, T. Liu, J. Liu, K. Liu and Y. Li, "Probabilistic power flow based on physics-guided graph neural networks," *Elect. Power Syst. Res.*, vol. 235, p. 110864, Oct. 2024.
- [11] N. Lin, S. Orfanoudakis, N. Ordóñez, J. Giraldo and P. Vergara, "Powerflownet: power flow approximation using message passing graph neural networks," *Int. J. Electr. Power Energy Syst.*, vol. 160, p. 110112, Sep. 2024.
- [12] Z. Hu, *et al.*, "Meteorological-electrical integrated real-time resilience assessment for power systems based on deep learning methods," *IEEE Trans. Smart Grid*, vol. 16, no. 5, pp. 3700-3713, Sep. 2025.
- [13] H. Li, L. Liu and Q. Wu, "Physics-guided chebyshev graph convolution network for optimal power flow," *Elect. Power Syst. Res.*, vol. 245, p. 111651, Aug. 2025.
- [14] Y. Li, *et al.*, "Data-physics joint-driven N-k static security assessment with higher-order graph convolution model," *Int. J. Electr. Power Energy Syst.*, vol. 172, p. 111128, Nov. 2025.
- [15] M. Gao, J. Yu, Z. Yang and J. Zhao, "Physics embedded graph convolution neural network for power flow calculation considering uncertain injections and topology," *IEEE Trans. Neural Netw. Learn. Syst.*, vol. 35, no. 11, pp. 15467-15478, Nov. 2024.
- [16] Y. Zhu, Y. Zhou, W. Wei, P. Li and W. Peng, "GNNs' generalization improvement for large-scale power system analysis based on physics-informed self-supervised pre-training," *IEEE Trans. Power Syst.*, vol. 40, no. 5, pp. 4145-4157, Sep. 2025.
- [17] J. Hansen, S. Anfin森 and F. Bianchi, "Power flow balancing with decentralized graph neural networks," *IEEE Trans. Power Syst.*, vol. 38, no. 3, pp. 2423-2433, May 2023.
- [18] V. Dwivedi, *et al.*, "Long range graph benchmark," in *Proc. Adv. Neural Inf. Process. Syst. (NeurIPS)*, vol. 35, pp. 22326-22340, 2022.
- [19] T. Chen, S. Yan, J. Guo and W. Wu, "ToupleGDD: a fine-designed solution of influence maximization by deep reinforcement learning," *IEEE Trans. Comput. Soc. Syst.*, vol. 11, no. 2, pp. 2210-2221, Apr. 2024.
- [20] H. Zeng, H. Zhou, A. Srivastava, R. Kannan, and V. Prasanna, "GraphSAINT: Graph sampling based inductive learning method," in *Proc. Int. Conf. Learn. Represent. (ICLR)*, 2020. [Online]. Available: <https://openreview.net/forum?id=BJe8pkHFwS>.
- [21] B. Huang, J. Wang, "Applications of physics-informed neural networks in power systems - a review," *IEEE Trans. Power Syst.*, vol. 38, no. 1, pp. 572-588, Jan. 2023.
- [22] T. Lopez-Garcia, J. Domínguez-Navarro, "Power flow analysis via typed graph neural networks," *Eng. Appl. Artif. Intell.*, vol. 117, p. 105567, Jan. 2023.
- [23] Y. Zhu, Y. Zhou, W. Wei and N. Wang, "Cascading failure analysis based on a physics-informed graph neural network," *IEEE Trans. Power Syst.*, vol. 38, no. 4, pp. 3632-3641, Jul. 2023.
- [24] J. Jalving, *et al.*, "Physics-informed machine learning with optimization-based guarantees: applications to ac power flow," *Int. J. Electr. Power Energy Syst.*, vol. 157, p. 109741, Jun. 2024.
- [25] J. Yang, Y. Xiang, "A virtual graph constrained learning method for power flow calculation," *IEEE Trans. Power Syst.*, vol. 39, no. 5, pp. 6784-6787, Sep. 2024.
- [26] S. Kirkland and S. Fallat, "Perron components and algebraic connectivity for weighted graphs," *Linear Multilinear Algebra*, vol. 44, no. 2, pp. 131-148, 1998.
- [27] A. Exposito, J. Ramos and J. Santos, "Slack bus selection to minimize the system power imbalance in load-flow studies," *IEEE Trans. Power Syst.*, vol. 19, no. 2, pp. 987-995, May 2004.
- [28] Q. Wu, *et al.*, "SGFormer: simplifying and empowering transformers for large-graph representations," in *Proc. Adv. Neural Inf. Process. Syst. (NeurIPS)*, vol. 36, pp. 64753-64773, 2023.
- [29] P. Veličković, G. Cucurull, A. Casanova, A. Romero, P. Liò, and Y. Bengio, "Graph attention networks," in *Proc. Int. Conf. Learn. Represent. (ICLR)*, 2018. [Online]. Available: <https://openreview.net/forum?id=rJXMpikCZ>.
- [30] A. Vaswani *et al.*, "Attention is all you need," in *Proc. Adv. Neural Inf. Process. Syst. (NeurIPS)*, vol. 30, 2017.